

# Carbon-supported and nanosheets-assembled vanadium oxide microspheres for stable lithium ion battery anodes

Chaojiang Niu<sup>§</sup>, Meng Huang<sup>§</sup>, Peiyao Wang<sup>§</sup>, Jiashen Meng, Xiong Liu, Xuanpeng Wang, Kangning Zhao, Yang Yu, Yuzhu Wu, Chao Lin, and Liqiang Mai (✉)

*Nano Res.*, **Just Accepted Manuscript** • DOI: 10.1007/s12274-015-0896-6  
<http://www.thenanoresearch.com> on September 10 2015

© Tsinghua University Press 2015

## Just Accepted

This is a “Just Accepted” manuscript, which has been examined by the peer-review process and has been accepted for publication. A “Just Accepted” manuscript is published online shortly after its acceptance, which is prior to technical editing and formatting and author proofing. Tsinghua University Press (TUP) provides “Just Accepted” as an optional and free service which allows authors to make their results available to the research community as soon as possible after acceptance. After a manuscript has been technically edited and formatted, it will be removed from the “Just Accepted” Web site and published as an ASAP article. Please note that technical editing may introduce minor changes to the manuscript text and/or graphics which may affect the content, and all legal disclaimers that apply to the journal pertain. In no event shall TUP be held responsible for errors or consequences arising from the use of any information contained in these “Just Accepted” manuscripts. To cite this manuscript please use its Digital Object Identifier (DOI®), which is identical for all formats of publication.

# **Carbon-supported and nanosheets-assembled vanadium oxide microspheres for stable lithium ion battery anodes**

Chaojiang Niu<sup>1</sup>, Meng Huang<sup>1</sup>, Peiyao Wang<sup>1</sup>, Jiashen Meng, Xiong Liu, Xuanpeng Wang,  
Kangning Zhao, Yang Yu, Yuzhu Wu, Chao Lin, Liqiang Mai\*

State Key Laboratory of Advanced Technology for Materials Synthesis and Processing,  
Wuhan University of Technology, Wuhan 430070, China

<sup>1</sup>These authors contributed equally to this work.

\*Corresponding author E-mail address: [mlq518@whut.edu.cn](mailto:mlq518@whut.edu.cn)

## **Abstract**

Transition metal oxides with high theoretical capacity and abundant source have attracted more interest than commercial graphite when used as anodes in lithium ion batteries. Construction of three-dimensional (3D) architectures decorated with conductive polymers and carbon is an efficient strategy to achieve excellent electrochemical performance for lithium ion battery electrodes. Herein, we have developed 3D carbon-supported amorphous vanadium oxide microspheres and crystalline V<sub>2</sub>O<sub>3</sub> microspheres via a facile solvothermal method. Both samples are assembled with ultrathin nanosheets, which consist of uniformly distributed vanadium oxides and carbon. The formation processes have been clearly illustrated and demonstrated through a series of time-dependent experiments. These specific microspheres have numerous active reaction sites, high electronic conductivity, and robust structural stability, showing great superiority among lithium ion battery anodes. Notably, when the amorphous microspheres are tested at the high rate of 2000 mA/g, 95% of the second cycle discharge capacity is maintained after cycling 7000 times. When the crystalline microspheres are tested at 2000 mA/g, 98% of the second cycle discharge capacity is remained after cycling 9000 times, demonstrating excellent high-rate and long-life performance. Therefore, this facile solvothermal method and unique carbon-supported and nanosheets-assembled microspheres have great potential and promising applications for lithium ion batteries.

**Keywords:** Vanadium oxide; microspheres; amorphous; lithium ion battery; anodes

## 1 Introduction

Owing to the high theoretical capacity and abundant source of raw materials, transition metal oxides have attracted more interest than commercial graphite when used as anodes in lithium ion batteries [1-18]. The ideal commercial electrodes also require both high rate and long lifespan characteristics to meet the booming needs of portable equipments [19-21]. To achieve these goals, nanotechnology has been widely studied and applied in both anodes and cathodes by many researchers on a worldwide scale. Nanostructures, including nanoparticles, nanowires, and nanosheets, have exhibited great superiority in lithium ion batteries because of their small size, accompanying with large specific surface area and short ion diffusion length [21-26]. However, the common and disastrous drawbacks of these low-dimensional nanostructures are self-aggregation and pulverization due to the large volume variation during the conversion reaction process, which have greatly limited their further applications [27]. Meanwhile, the low electronic conductivity of transition metal oxide also severely weakens its rate performance.

To overcome these above-mentioned problems, many efforts have been focused on developing various three-dimensional (3D) nanostructures to improve the structural stability and electrochemical performance [28-36]. Jeong et al. reported a 3D hierarchical core-shell hollow structure of  $\text{Fe}_2\text{O}_3@\text{PANI}$ , which yielded robust electrochemical performance when used as an anode [11]. Coating conductive polymers or carbon is also an effective approach to enhance the performance of anodes. Luo et al. developed bicontinuous mesoporous  $\text{Fe}_3\text{O}_4$  nanostructures on 3D graphene foams, exhibiting long cycle life and high rate performance when used as lithium battery anodes [36]. Therefore, it is of great benefit and significance to combine these two merits together for highly improved lithium ion batteries.

Vanadium oxides, among the focused transition metal oxides, have been widely investigated due to their high capacity and abundant source in lithium ion batteries [37-41]. For  $\text{V}_2\text{O}_5$ , when the  $\text{V}^{5+}$  is reduced to the  $\text{V}^0$ , it presents a high theoretical

capacity of 1472 mAh/g as an anode in a lithium ion battery [42-46]. Therefore, vanadium oxides are ideal candidates for high capacity electrodes. However, the structural degradation, poor electrochemical kinetics and low electronic conductivity, have seriously confined their further developments. Sun et al. coated graphene on amorphous vanadium oxides via an atomic layer deposition method to enhance electronic conductivity and electrochemical activity [42]. Augustyn and Dunn reported that vanadium oxide aerogels with high surface area and mesoporous architecture could efficiently accommodate large volume variation and exhibit large reversible capacities [43]. Chae et al. reported that amorphous  $V_2O_5$  with highly populated vacant sites possesses good rate capability and high reversible capacity, owing to the easy access of lithium ions and the lack of interactions between the inserted ions/electrons and  $V_2O_5$  matrix [47]. Therefore, 3D nanostructures combined with carbon coating will be an effective way to take full advantages of vanadium oxides and achieve high-rate and long-life lithium ion batteries [48-58].

In this work, we synthesized carbon-supported amorphous vanadium oxide microspheres and crystalline  $V_2O_3$  microspheres through a feasible solvothermal method followed by heat treatment. The formation processes have also been clearly illustrated through a series of time-dependent experiments. Both of the microspheres are assembled with ultrathin nanosheets, which consist of uniformly distributed carbon and vanadium oxides. These nanostructures exhibiting the characteristics of low charge transfer resistance, high electronic transport, large surface area and robust structural stability, will have great superiority when used as lithium ion battery anodes.

## 2 Experimental

### 2.1 Materials synthesis

**Preparation of amorphous vanadium oxide microspheres:** All commercial chemicals or materials were used directly without any further purification. In a typical synthesis, 0.28 g ammonium metavanadate and 0.50 g citric acid were dissolved into the mixed solvent of ethanediol (30 mL) and deionized water (10 mL), to obtain light

yellow solution. Then the solution was stirred for 5 h at 60 °C, until the solution turned atrovirens. Then it was transferred into a 50 mL Teflon autoclave and kept at 180 °C for different reaction times. After naturally cooling to ambient temperature, the precipitates were washed mildly by pure alcohol and deionized water for several times, and dried at 70 °C in air for 12 h. At last, the samples were obtained after heating at 150 °C for 5 h in nitrogen atmosphere.

**Preparation of crystalline V<sub>2</sub>O<sub>3</sub> microspheres:** The preliminary process is the same with that mentioned above. After drying in air, the products were sintered at 600 °C for 3 h in nitrogen atmosphere to get final samples.

## 2.2 Characterization

X-ray diffraction (XRD) measurements were measured using a Bruker D8 Discover X-ray diffractometer equipped with a Cu K $\alpha$  radiation source; the samples were scanned at room temperature (the 2 $\theta$  ranges from 10° to 80°). Field emission scanning electron microscopy (SEM) images were collected using a JEOL-7100F scanning electron microscope. Transmission electron microscopy (TEM) images were collected using a JEM-2100F microscope. Energy-dispersive X-ray spectra (EDS) were recorded using an Oxford IE250 system. Brunauer-Emmett-Teller (BET) surface area was calculated from nitrogen adsorption isotherms measured at 77 K using a Tristar-3020 instrument. X-ray photoelectron spectroscopy (XPS) measurements were obtained using a VG MultiLab 2000 instrument. Thermogravimetric–DSC analyses (TG-DSC) were conducted using a STA-449C.

## 2.3 Measurements of electrochemical performance

The 2016 coin cells were assembled in a glovebox filled with pure argon. Lithium foil was used as the anode and a solution of LiPF<sub>6</sub> (1 M) in ethylene carbonate (EC)/dimethylcarbonate (DMC) (1:1 vol/vol) was used as the electrolyte. The working electrode was composed of a ground mixture of 70% active material, 20% acetylene black and 10% poly(tetrafluoroethylene) (PTFE). **After coating onto copper foil, the electrode film was uniformly cut into round slice with ~0.5 cm<sup>2</sup> in area and ~1.2 mg in weight, the areal mass loading is 2.4 mg/(cm)<sup>2</sup>.** Galvanostatic charge/discharge measurements were performed in the potential range of 0.01-3 V vs.

Li/Li<sup>+</sup> using a multichannel battery testing system (LAND CT2001A). Cyclic voltammetry (CV) were collected at room temperature using an Autolab potentiostat/galvanostat (Autolab PGSTAT 302).

### 3 Results and Discussion

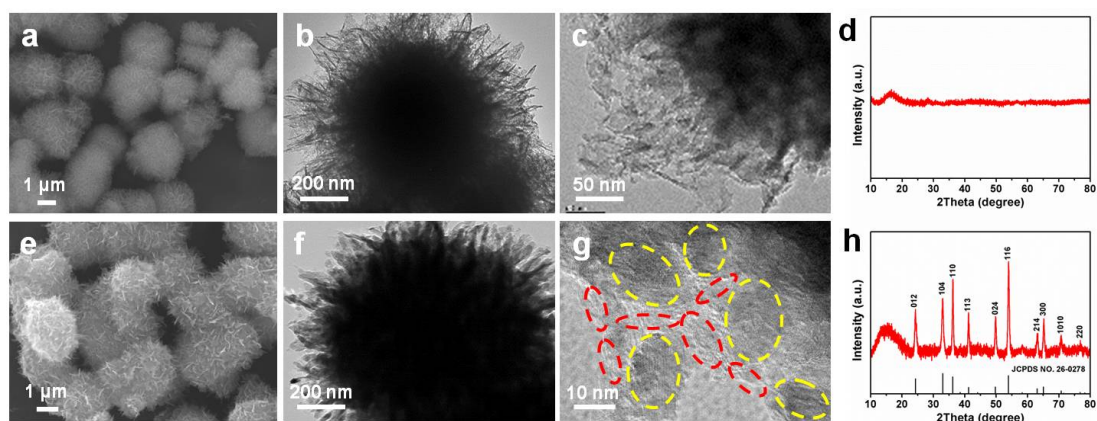


**Figure 1.** SEM image (a), TEM images (b-c), and XRD pattern (d) of amorphous vanadium oxide microspheres. SEM image (e), TEM images (f-g), and XRD pattern (h) of crystalline V<sub>2</sub>O<sub>3</sub> microspheres. The red cycle represents carbon and the yellow cycle represents V<sub>2</sub>O<sub>3</sub> in the TEM image of (g).

Carbon-supported and nanosheets-assembled amorphous vanadium oxide microspheres are synthesized via a facile solvothermal method with subsequent heat treatment. As shown in the SEM and TEM images, both amorphous vanadium oxide and crystalline V<sub>2</sub>O<sub>3</sub> are uniform microspheres assembled with ultrathin nanosheets (Fig. 1). The diameter of each microsphere is ~2 μm and the nanosheets are homogeneous with ~10 nm in thickness. The amorphous vanadium oxide microspheres, prepared at a low temperature of 150 °C in nitrogen, are demonstrated by the high resolution TEM image (Fig. 1c) and the typical XRD pattern (Fig. 1d). Then the crystalline microspheres, which can be indexed to the rhombohedral-phase crystalline V<sub>2</sub>O<sub>3</sub> without detectable impurity (JCPDS No. 26-0278), are fabricated after sintering at high temperature of 600 °C in nitrogen atmosphere. Furthermore, the

microsphere nanostructure has also been perfectly maintained after high temperature sintering in air, demonstrating great structural stability (Figure S1, in the Electronic Supplementary Materials (ESM)).

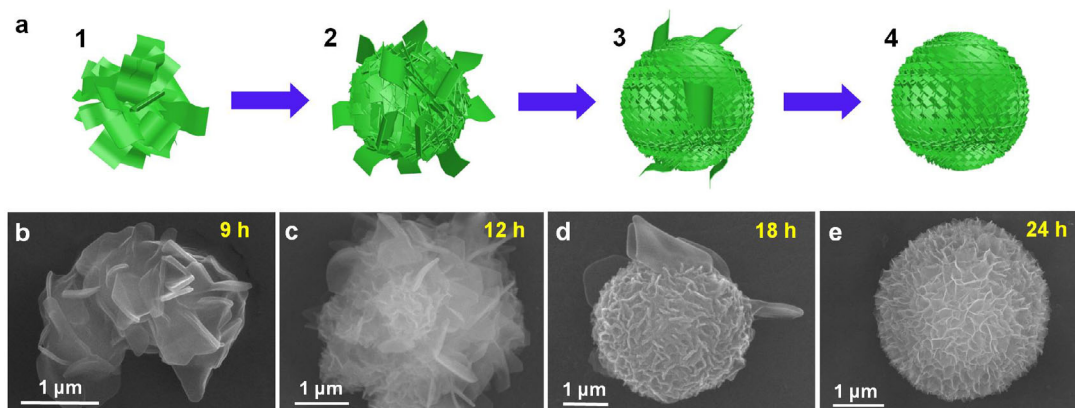


**Figure 2.** (a) Schematic of the formation process of carbon-supported and nanosheets-assembled amorphous vanadium oxide microspheres. (b-e) SEM images of the samples prepared at 9 h (b), 12 h (c), 18 h (d) and 24 h (e), respectively.

To further understand the formation processes of microspheres, a series of time-dependent experiments are carried out. Four samples with different morphologies were synthesized with the reacting time increasing from 9 to 12, 18 and 24 h (Fig. 2). When the reaction time was only 9 h, tanglesome thick vanadium oxide nanosheets were initially obtained, which aggregated together owing to the tendency of decreasing surface energy (Fig. 2b). Then as the reacting time increased to 12 h, the thick vanadium oxide nanosheets were gradually consumed and ultrathin vanadium oxide nanosheets were gradually formed (Fig. 2c). After reacting for 18 h, the transformation continued to proceed, forming homogeneous microspheres (Fig. 2d). Finally, vanadium oxide microspheres assembled with nanosheets were synthesized after reacting for 24 h (Fig. 2e). All these four corresponding XRD patterns demonstrate the amorphous characteristic of the samples (Fig. S2, in the ESM). And each pattern also exhibits an obvious weak and broad diffraction peak at about  $17^\circ$ , indicating that the carbon layers are formed throughout the formation process and in

situ cover on the vanadium oxide nanosheets, which can also be proved by the TEM image (Fig. 1g). The EDS elemental mapping image also proves the uniform distribution of the carbon, which is derived from the decomposition and carbonization of ethanediol and citric acid (Fig. S3, in the ESM). Then the Raman spectrum is measured to study the characteristics of carbon in crystalline  $V_2O_3$  microspheres (Fig. S4, in the ESM). The characteristic signatures are observed at  $\sim 1350$  and  $\sim 1600\text{ cm}^{-1}$ , corresponding to the D-band (originating from disordered carbon) and G-band (graphitic carbon), respectively. The intensity ratio of D-band to G-band ( $I_D/I_G$  value) is 1.04, indicating the partially graphitization of carbon [59]. The TG-DSC curves show the mass percentage of carbon is  $\sim 10.6\text{ wt}\%$  in amorphous vanadium oxide microspheres and  $\sim 8.1\text{ wt}\%$  in crystalline  $V_2O_3$  microspheres (Fig. S5, in the ESM).

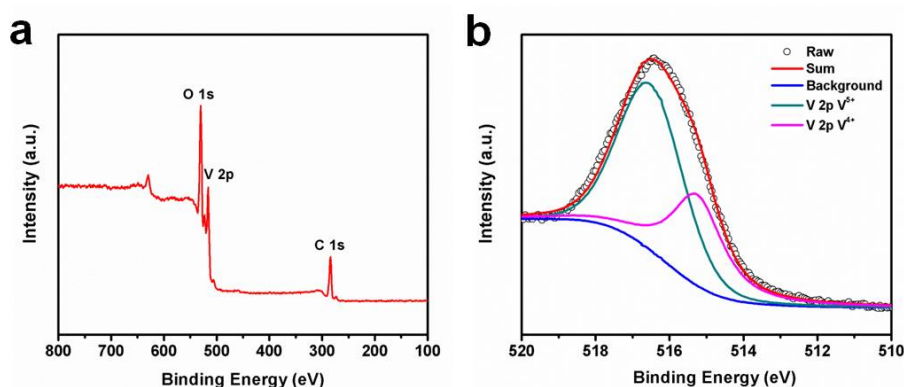


**Figure 3.** (a) XPS spectra and (b) V  $2p_{3/2}$  XPS spectra of carbon-supported and nanosheets-assembled amorphous vanadium oxide microspheres.

Then the elaborate architectures and compositions of the above carbon-supported and nanosheets-assembled amorphous vanadium oxide microspheres are further studied. XPS measurement was carried out to reveal the valence states of the elements in amorphous vanadium oxide microspheres (Fig. 3). All peaks correspond to vanadium, oxygen, and carbon in the survey-scan XPS, which are consistent with the EDS elemental mapping measurement. The V  $2p_{3/2}$  core peak spectrum for amorphous vanadium oxide microspheres is composed of two components located at 516.80 and 515.60 eV, corresponding to two formal oxidation states (+5 and +4), respectively,

and their ratio is  $\sim 2:1$ . Therefore, the vanadium-to-oxygen molar ratio is  $\sim 3:7$ , close to the EDS characterization value (3:7.08). The specific surface area of amorphous vanadium oxide microspheres is measured as  $28 \text{ m}^2/\text{g}$ , and the Barrett-Joyner-Halenda (BJH) pore-size distribution curve displays no obvious pores (Fig. S6, in the ESM). Nevertheless, after sintering at high temperature of  $600 \text{ }^\circ\text{C}$  in nitrogen, carbon-supported and nanosheets-assembled crystalline  $\text{V}_2\text{O}_3$  microspheres were obtained and exhibited a greatly increased specific surface area of  $45 \text{ m}^2/\text{g}$ . This is mainly attributed to the formation of mesopores in the crystalline  $\text{V}_2\text{O}_3$  microspheres. The BJH pore-size distribution curve manifests that the diameter of the new pores is  $\sim 20 \text{ nm}$ , belonging to mesopores, which can effectively increase the electrode/electrolyte contact area and shorten the path length for ionic/electronic transport.

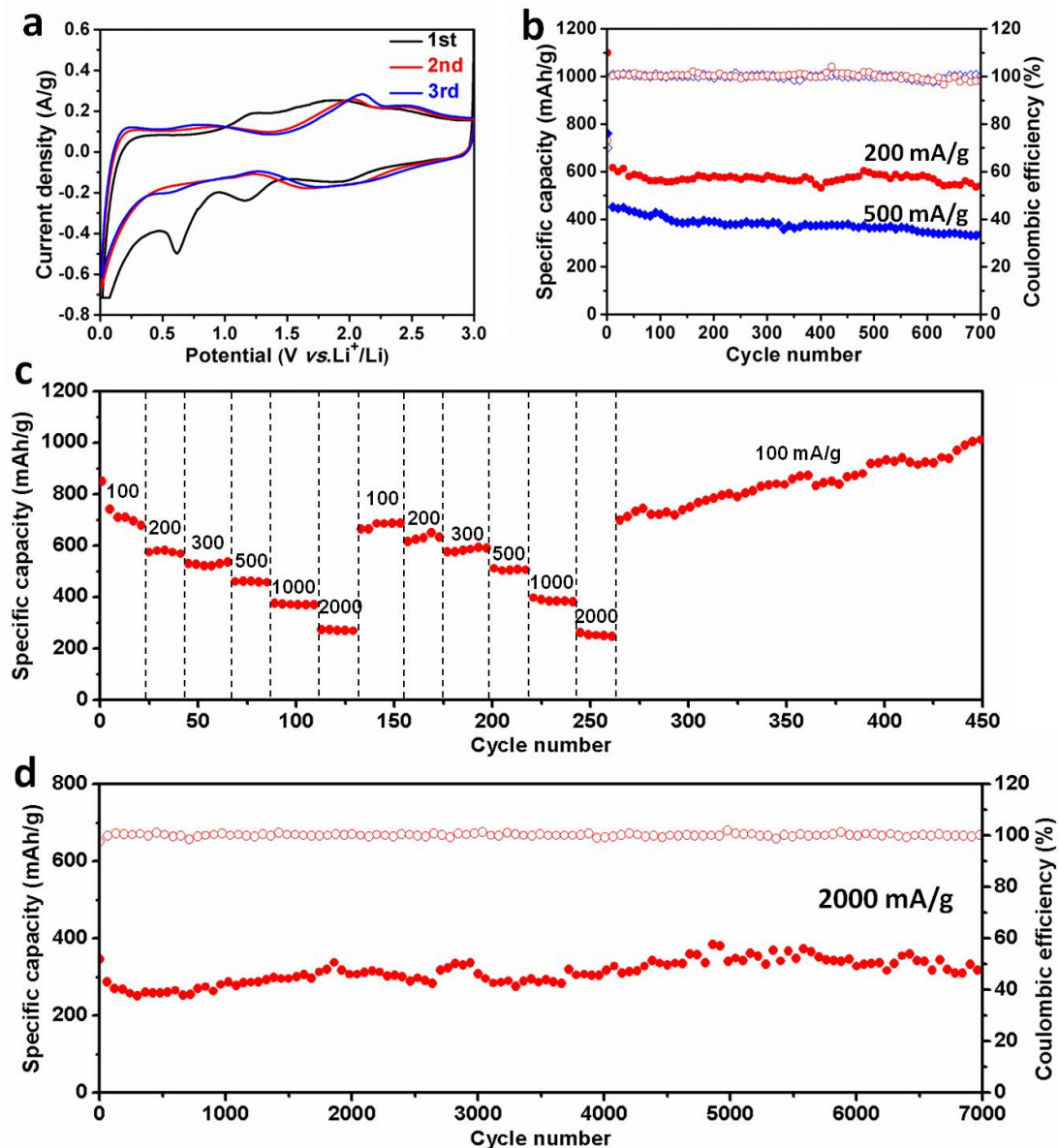


**Figure 4.** Electrochemical performance of carbon-supported and nanosheets-assembled amorphous vanadium oxide microspheres. (a) The first three CV curves tested at a scan rate of 0.2 mV/s in the potential range from 0.01 to 3.0 V vs  $\text{Li}/\text{Li}^+$ . (b) Cycling performance and the corresponding coulombic efficiencies are tested at the current densities of 200 and 500 mA/g, respectively. (c) Rate performance tested from 100 to 200, 300, 500, 1000 and 2000 mA/g, respectively. (d) Cycling performance and coulombic efficiency tested at the high current density of 2000 mA/g.

To reveal the superiority of carbon-supported amorphous vanadium oxide microspheres and crystalline  $\text{V}_2\text{O}_3$  microspheres, the electrochemical performance is

characterized. First, the CV measurement of amorphous vanadium oxide microspheres is performed to characterize the phase transformation process during charge/discharge reactions between 0.01 V and 3 V at a scan rate of 0.2 mV/s (Fig. 4a). For the first discharge cycle, three reduction peaks at 1.98, 1.21 and 0.61 V can be related to the formation of  $\text{Li}_y\text{VO}_x$  new phases and solid-electrolyte interphase (SEI) on the surface of active materials. While both the second and the third curves show broad peaks and overlap mostly, indicating good reversibility of electrochemical reactions. It is well known that the lithium storage of vanadium oxide is mainly attributed to the intercalation and conversion reactions. In previous report, vanadium oxides first undergo the intercalation reaction, forming new phases of  $\text{VO}_x$ , and then followed by the conversion reaction, forming  $\text{V}_2\text{O}$ . Therefore, amorphous vanadium oxide is expected to reveal a theoretical capacity of over 900 mAh/g [43-47].

Then the cycling performance of amorphous vanadium oxide microspheres is tested at a low current density of 100 mA/g, it exhibits a high discharge capacity of 1347 mAh/g for the first cycle and 800 mAh/g for the second cycle, and the coulombic efficiency for the first cycle is 65% (Fig. S7a, in the ESM). When it is measured at the current densities of 200 and 500 mA/g, 84% and 71% of the second cycle discharge capacities (668 and 488 mAh/g) are maintained after cycling 700 times, respectively (Fig. 4b). The rate performance is measured at various rates ranging from 100 to 200, 300, 500, 1000 and 2000 mA/g, respectively (Fig. 4c). The capacity recovery exceeds 100% when the current density is reduced to 100 mA/g and the discharge capacity increases obviously in the subsequent measurement. And the corresponding charge-discharge curves also demonstrate high coulombic efficiency (Fig. S7b, in the ESM). Particularly, when tested at the high current density of 2000 mA/g, amorphous vanadium oxide microspheres maintain 95% of the second cycle capacity (345 mAh/g) after cycling a long lifespan of 7000 times, demonstrating excellent cycling performance (Fig. 4d).

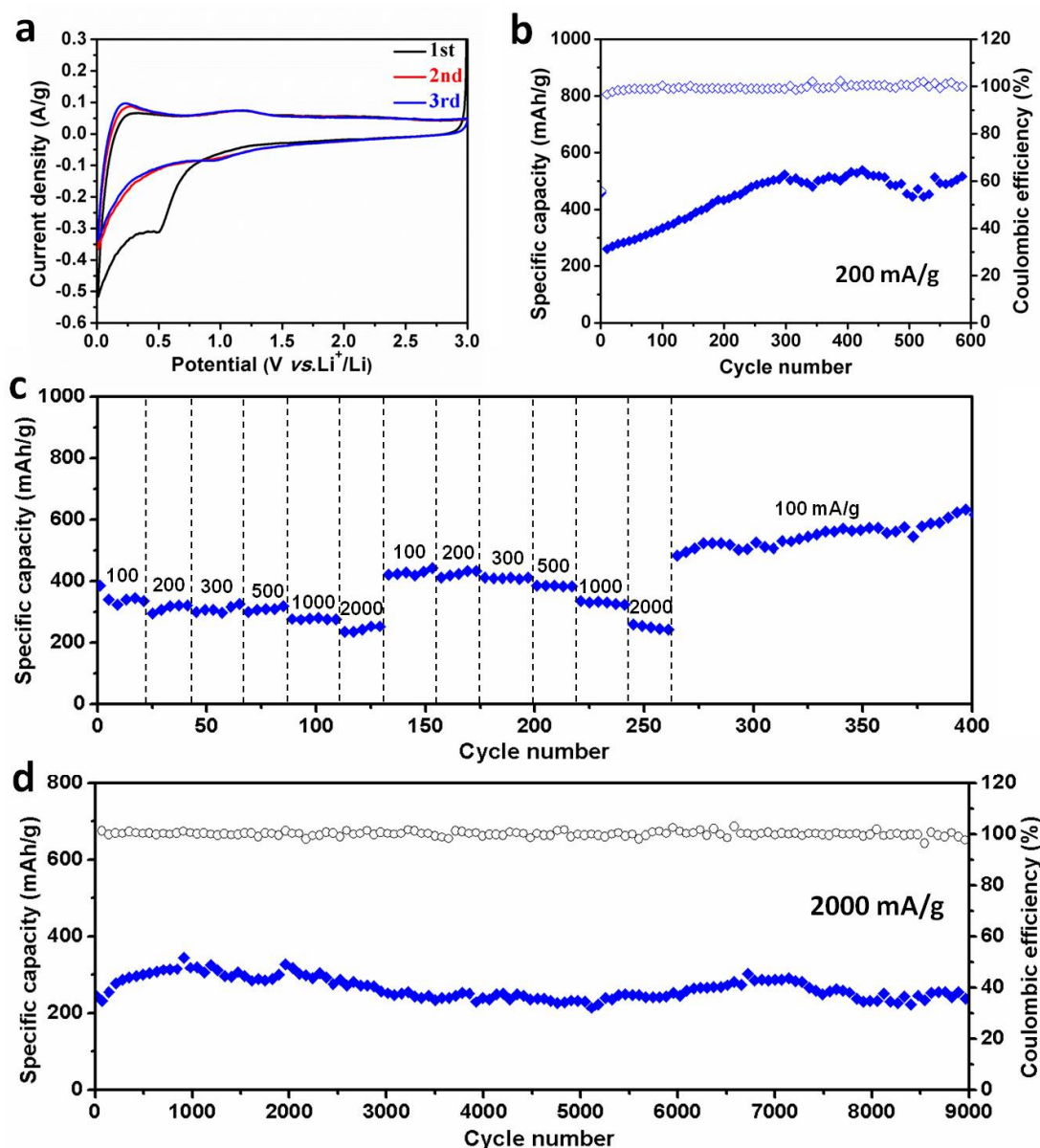


**Figure 5.** Electrochemical performance of carbon-supported and nanosheets-assembled crystalline  $V_2O_3$  microspheres. (a) The first three CV curves tested at a scan rate of 0.2 mV/s in a potential range from 0.01 to 3.0 V vs  $Li/Li^+$ . (b) Cycling performance tested at the current density of 200 mA/g. (c) Rate performance tested from 100 to 200, 300, 500, 1000 and 2000 mA/g, respectively. (d) Cycling performance at the high current density of 2000 mA/g.

Then the electrochemical performance of carbon-supported and nanosheets-assembled crystalline  $V_2O_3$  microspheres is further characterized. The first three consecutive CV curves of  $V_2O_3$  microspheres are carried out to characterize the phase transformation process during charge/discharge reactions between 0.01 V and 3

V at a scan rate of 0.2 mV/s (Fig. 5a). Compared to the results of amorphous vanadium oxide microspheres measured above, the number of reduction and oxidation peaks obviously decreases, since the highest valence state of vanadium is only +3 during the electrochemical reactions. The valence state of vanadium only changes from +1 to +3 under the voltage of 1.5 V, and no peaks are observed above 1.5 V for the first three CV curves. Therefore, the specific discharge capacity of crystalline  $V_2O_3$  microspheres is lower than that of amorphous vanadium oxide microspheres. When it is tested at a low current density of 200 mA/g, the coulombic efficiency for the first cycle is 56%, the discharge capacity gradually increases for the first 300 cycles and remains stable for the subsequent measurement (Fig. 5b). The 600<sup>th</sup> cycle discharge capacity is 505 mAh/g and the corresponding coulombic efficiency remains at ~100%, indicating a good reversibility. The increased capacity has also been widely observed for other transition metal oxides, which is attributed to the electrochemical activation and the growth of an electrochemical gel-like polymer layer [56-63]. The rate performance is tested at various rates ranging from 100 to 200, 300, 500, 1000 and 2000 mA/g, corresponding to the average discharge capacities of 341, 321, 318, 310, 279 and 245 mAh/g, respectively (Fig. 5c). When the current density comes back to 100 mA/g, the capacity recovery exceeds 100% and the 400<sup>th</sup> cycle discharge capacity reaches up to 621 mAh/g, showing great reversibility. Notably, when crystalline  $V_2O_3$  microspheres are tested at the high current density of 2000 mA/g, 98% of the second cycle discharge capacity is still maintained after cycling as long as 9000 times, demonstrating excellent high-rate and long-life performance (Fig. 5d).

Based on the measurements above, the outstanding electrochemical performance of carbon-supported amorphous vanadium oxide and crystalline  $V_2O_3$  microspheres can be attributed to the following reasons. First, both microspheres are assembled with ultrathin nanosheets and have a large specific surface area, which can shorten the path length for ionic/electronic transport and enhance the electrode/electrolyte contact area. The specific surface area of amorphous vanadium oxide microspheres is 28 m<sup>2</sup>/g, and the crystalline  $V_2O_3$  microspheres exhibit a much higher value of 45 m<sup>2</sup>/g after high temperature sintering in nitrogen (Fig. S6, in the ESM). Second, the existence of

graphitized carbon can effectively increase the conductance of the microspheres and reduce the charge transfer resistance ( $R_{ct}$ ). The electrochemical impedance spectroscopy (EIS) measurement shows that the  $R_{ct}$  values of carbon-supported amorphous vanadium oxide microspheres and crystalline  $V_2O_3$  microspheres are 92  $\Omega$  and 51  $\Omega$ , respectively, indicating high electronic conductivity and enhanced kinetics of the electrode reactions (Fig. S4a, in the ESM). Third, the unique microsphere structure assembled with ultrathin nanosheets can restrain the self-aggregation and release the stress caused by volume variation during the lithium ion intercalation and deintercalation processes. After charging and discharging 400 cycles at 200 mA/g, the 3D nanostructures of both amorphous vanadium oxide microspheres and crystalline  $V_2O_3$  microspheres are kept integrity (Fig. S8, in the ESM), showing great structural stability. All these results demonstrate that our carbon-supported amorphous vanadium oxide and crystalline  $V_2O_3$  microspheres are promising anodes in high-rate and long-life lithium batteries (Table S1).

#### **4 Conclusions**

In this work, we have developed a facile solvothermal method to synthesize 3D carbon-supported microspheres, including amorphous vanadium oxides and crystalline  $V_2O_3$ , which are assembled with ultrathin nanosheets. Both of them exhibit excellent high-rate and long-life electrochemical performance when used as lithium ion battery anodes. The amorphous vanadium oxide microspheres exhibit a little higher discharge capacities and the crystalline  $V_2O_3$  microspheres show a bit better cycling performance. Particularly, when carbon-supported amorphous vanadium oxide microspheres are tested at the high current density of 2000 mA/g, 95% of the second cycle discharge capacity is maintained after cycling as long as 7000 times. When crystalline  $V_2O_3$  microspheres are tested at 2000 mA/g, 98% of the second cycle discharge capacity is remained after cycling an ultra-long life of 9000 times. This excellent cycling performance mainly benefits from the uniformly distributed carbon and the stable microsphere structure, which is accompanied with low charge transfer resistance, fast electronic transport, large specific surface area and robust

structural stability. Therefore, these carbon-supported and nanosheets-assembled microsphere anodes have enormous potential in the energy storage field.

### Acknowledgements

This work was supported by the National Basic Research Program of China (2013CB934103, 2012CB933003), the International Science & Technology Cooperation Program of China (2013DFA50840), the National Natural Science Foundation of China (51302203, 51272197), the National Natural Science Fund for Distinguished Young Scholars (51425204), the Hubei Province Natural Science Fund for Distinguished Young Scholars (2014CFA035), the Fundamental Research Funds for the Central Universities (WUT: 2013-ZD-7, 2014-VII-007) and the Students Innovation and Entrepreneurship Training Program (2014-CL-A1-01, 2015-CL-B1-23). We thank Prof. D. Y. Zhao of Fudan University for useful discussions and assistance with the manuscript.

### References

- [1] Armand, M.; Tarascon, J. M. Building better batteries. *Nature* **2008**, *451*, 652-657.
- [2] Reddy, M. V.; Subba Rao, G. V.; Chowdari, B. V. R. Metal oxides and oxysalts as anode materials for Li ion batteries. *Chem. Rev.* **2013**, *113*, 5364-5457.
- [3] Liu, Y. X.; Wang, D. S.; Peng, Q.; Chu, D. R.; Liu, X. W.; Li, Y. D. Directly assembling ligand-free ZnO nanocrystals into three-dimensional mesoporous structures by oriented attachment. *Inorg. Chem.* **2011**, *50*, 5841-5847.
- [4] Poizot, P.; Laruelle, S.; Grugeon, S.; Dupont, L.; Tarascon, J. M. Nano-sized transition-metal oxides as negative-electrode materials for lithium-ion batteries. *Nature* **2000**, *407*, 496-499.
- [5] Armstrong, M. J.; O'Dwyer, C.; Macklin, W. J.; Holmes, J. D. Evaluating the performance of nanostructured materials as lithium-ion battery electrodes. *Nano Res.* **2014**, *7*, 1-62.
- [6] Liu, B.; Zhang, J.; Wang, X. F.; Chen, G.; Chen, D.; Zhou, C. W.; Shen, G. Z. Hierarchical three-dimensional ZnCo<sub>2</sub>O<sub>4</sub> nanowire arrays/carbon cloth anodes for a novel class of high-performance flexible lithium-ion batteries. *Nano Lett.* **2012**, *12*, 3005-3011.
- [7] Zhou, L.; Zhao, D. Y.; Lou, X. W. LiNi<sub>0.5</sub>Mn<sub>1.5</sub>O<sub>4</sub> hollow structures as high-performance cathodes for lithium-ion batteries. *Angew. Chem. Int. Ed.* **2012**, *51*, 239-241.
- [8] Wu, H. B.; Chen, J. S.; Hng, H. H.; Lou, X. W. Nanostructured metal oxide-based materials as

- advanced anodes for lithium-ion batteries. *Nanoscale* **2012**, *4*, 2526-2542.
- [9] Wei, Q. L.; Tan, S. S.; Liu, X. Y.; Yan, M. Y.; Wang, F. C.; Li, Q. D.; An, Q. Y.; Sun, R. M.; Zhao, K. N.; Wu, H. A.; Mai, L. Q. Novel polygonal vanadium oxide nanoscrolls as stable cathode for lithium storage. *Adv. Funct. Mater.* **2015**, *25*, 1773-1779.
- [10] He, C. N.; Wu, S.; Zhao, N. Q.; Shi, C. S.; Liu, E. Z.; Li, J. J. Carbon-encapsulated Fe<sub>3</sub>O<sub>4</sub> nanoparticles as a high-rate lithium ion battery anode material. *ACS Nano* **2013**, *7*, 4459-4469.
- [11] Jeong, J. M.; Choi, B. G.; Lee, S. C.; Lee, K. G.; Chang, S. J.; Han, Y. K.; Lee, Y. B.; Lee, H. U.; Kwon, S.; Lee, G. et al. Hierarchical hollow spheres of Fe<sub>2</sub>O<sub>3</sub>@polyaniline for lithium ion battery anodes. *Adv. Mater.* **2013**, *25*, 6250-6255.
- [12] Wang, L. J.; Zhang, K.; Hu, Z.; Duan, W. C.; Cheng, F. Y.; Chen, J. Porous CuO nanowires as the anode of rechargeable Na-ion batteries. *Nano Res.* **2014**, *7*, 199-208.
- [13] Lee, C. W.; Seo, S. D.; Kim, D. W.; Park, S.; Jin, K.; Kim, D. W.; Hong, K. S. Heteroepitaxial growth of ZnO nanosheet bands on ZnCo<sub>2</sub>O<sub>4</sub> submicron rods toward high-performance Li ion battery electrodes. *Nano Res.* **2013**, *6*, 348-355.
- [14] Jian, Z. L.; Zheng, M. B.; Liang, Y. L.; Zhang, X. X.; Gheytani, S.; Lan, Y. C.; Shi, Y.; Yao, Y. Li<sub>3</sub>VO<sub>4</sub> anchored graphene nanosheets for long-life and high-rate lithium-ion batteries. *Chem. Commun.* **2015**, *51*, 229-231.
- [15] Su, D. W.; Dou, S. X.; Wang, G. X. Mesocrystal Co<sub>3</sub>O<sub>4</sub> nanoplatelets as high capacity anode materials for Li-ion batteries. *Nano Res.* **2014**, *7*, 794-803.
- [16] Xie, R. G.; Li, Z.; Peng, X. G. Nucleation kinetics vs chemical kinetics in the initial formation of semiconductor nanocrystals. *J. Am. Chem. Soc.* **2009**, *131*, 15457-15466.
- [17] Chen, Y.; Song, B. H.; Li, M.; Lu, L.; Xue, J. M. Fe<sub>3</sub>O<sub>4</sub> nanoparticles embedded in uniform mesoporous carbon spheres for superior high-rate battery applications. *Adv. Funct. Mater.* **2014**, *24*, 319-326.
- [18] Ji, X. L.; Lee, K. T.; Nazar, L. F. A highly ordered nanostructured carbon-sulphur cathode for lithium-sulphur batteries. *Nat. Mater.* **2009**, *8*, 500-506.
- [19] Chen, P. C.; Xu, J.; Chen, H. T.; Zhou, C. W. Hybrid silicon-carbon nanostructured composites as superior anodes for lithium ion batteries. *Nano Res.* **2011**, *4*, 290-296.
- [20] Palacin, M. R. Recent advances in rechargeable battery materials: A chemist's perspective. *Chem. Soc. Rev.* **2009**, *38*, 2565-2575.

- [21] Niu, C. J.; Meng, J. S.; Wang, X. P.; Han, C. H.; Yan, M. Y.; Zhao, K. N.; Xu, X. M.; Ren, W. H.; Zhao, Y. L.; Xu, L. et al. General synthesis of complex nanotubes by gradient electrospinning and controlled pyrolysis. *Nat. Commun.* **2015**, *6*, 7402.
- [22] Yao, J.; Yan, H.; Lieber, C. M. A nanoscale combing technique for the large-scale assembly of highly aligned nanowires. *Nat. Nanotechnol.* **2013**, *8*, 329-335.
- [23] Wu, H.; Zheng, G. Y.; Liu, N.; Carney, T. J.; Yang, Y.; Cui, Y. Engineering empty space between Si nanoparticles for lithium-ion battery anodes. *Nano Lett.* **2012**, *12*, 904-909.
- [24] Magasinski, A.; Dixon, P.; Hertzberg, B.; Kvit, A.; Ayala, J.; Yushin, G. High-performance lithium-ion anodes using a hierarchical bottom-up approach. *Nat. Mater.* **2010**, *9*, 353-358.
- [25] Yan, X. Q.; Wang, X. J.; Tang, Y.; Ma, G. C.; Zou, S. H.; Li, R. H.; Peng, X. G.; Dai, S.; Fan, J. Unusual loading-dependent sintering-resistant properties of gold nanoparticles supported within extra-large mesopores. *Chem. Mater.* **2013**, *25*, 1556-1563.
- [26] Zhou, W. J.; Cao, X. H.; Zeng, Z. Y.; Shi, W. H.; Zhu, Y. Y.; Yan, Q. Y.; Liu, H.; Wang, J. Y.; Zhang, H. One-step synthesis of Ni<sub>3</sub>S<sub>2</sub> nanorod@Ni(OH)<sub>2</sub> nanosheet core-shell nanostructures on a three-dimensional graphene network for high-performance supercapacitors. *Energy Environ. Sci.* **2013**, *6*, 2216-2221.
- [27] Mai, L. Q.; Tian, X. C.; Xu, X.; Chang, L.; Xu, L. Nanowire electrodes for electrochemical energy storage devices. *Chem. Rev.* **2014**, *114*, 11828-11862.
- [28] Zhang, H. G.; Yu, X. D.; Braun, P. V. Three-dimensional bicontinuous ultrafast charge and discharge bulk battery electrodes. *Nat. Nanotechnol.* **2011**, *6*, 277-281.
- [29] Qiu, Y. C.; Xu, G. L.; Kuang, Q.; Sun, S. G.; Yang, S. H. Hierarchical WO<sub>3</sub> flowers comprising porous single-crystalline nanoplates show enhanced lithium storage and photocatalysis. *Nano Res.* **2012**, *5*, 826-832.
- [30] Liu, N.; Lu, Z. D.; Zhao, J.; McDowell, M. T.; Lee, H. W.; Zhao, W. T.; Cui, Y. A pomegranate-inspired nanoscale design for large-volume-change lithium battery anodes. *Nat. Nanotechnol.* **2014**, *9*, 187-192.
- [31] Liang, Y. Y.; Li, Y. G.; Wang, H. L.; Dai, H. J. Strongly coupled inorganic/nanocarbon hybrid materials for advanced electrocatalysis. *J. Am. Chem. Soc.* **2013**, *135*, 2013-2036.
- [32] Xu, Y. X.; Huang, X. Q.; Lin, Z. Y.; Zhong, X.; Huang, Y.; Duan, X. F. One-step strategy to graphene/Ni(OH)<sub>2</sub> composite hydrogels as advanced three-dimensional supercapacitor electrode

materials. *Nano Res.* **2013**, *6*, 65-76.

[33] Li, L.; Lu, H.; Yang, Z. Y.; Tong, L. M.; Bando, Y.; Golberg, D. Bandgap-graded CdS<sub>x</sub>Se<sub>1-x</sub> nanowires for high-performance field-effect transistors and solar cells. *Adv. Mater.* **2013**, *25*, 1109-1113.

[34] Chen, S. Q.; Bao, P. T.; Huang, X. D.; Sun, B.; Wang, G. X. Hierarchical 3D mesoporous silicon@graphene nanoarchitectures for lithium ion batteries with superior performance. *Nano Res.* **2014**, *7*, 85-94.

[35] Liu, X. Q.; Wang, C. L.; Cai, B.; Xiao, X. H.; Guo, S. S.; Fan, Z. Y.; Li, J. C.; Duan, X. F.; Liao, L. Rational design of amorphous indium zinc oxide/carbon nanotube hybrid film for unique performance transistors. *Nano Lett.* **2012**, *12*, 3596-3601.

[36] Luo, J. S.; Liu, J. L.; Zeng, Z. Y.; Ng, C. F.; Ma, L. J.; Zhang, H.; Lin, J. Y.; Shen, Z. X.; Fan, H. J. Three-dimensional graphene foam supported Fe<sub>3</sub>O<sub>4</sub> lithium battery anodes with long cycle life and high rate capability. *Nano Lett.* **2013**, *13*, 6136-6143.

[37] Niu, C. J.; Meng, J. S.; Han, C. H.; Zhao, K. N.; Yan, M. Y.; Mai, L. Q. VO<sub>2</sub> nanowires assembled into hollow microspheres for high-rate and long-life lithium batteries. *Nano Lett.* **2014**, *14*, 2873-2878.

[38] Sheng, J. Z.; Li, Q. D.; Wei, Q. L.; Zhang, P. F.; Wang, Q. Q.; Lv, F.; An, Q. Y.; Chen, W.; Mai, L. Q. Metastable amorphous chromium-vanadium oxide nanoparticles with superior performance as a new lithium battery cathode. *Nano Res.* **2014**, *7*, 1604-1612.

[39] An, Q. Y.; Zhang, P. F.; Xiong, F. Y.; Wei, Q. L.; Sheng, J. Z.; Wang, Q. Q.; Mai, L. Q. Three-dimensional porous V<sub>2</sub>O<sub>5</sub> hierarchical octahedrons with adjustable pore architectures for long-life lithium batteries. *Nano Res.* **2015**, *8*, 481-490.

[40] Pan, A. Q.; Wu, H. B.; Yu, L.; Lou, X. W. Template-free synthesis of VO<sub>2</sub> hollow microspheres with various interiors and their conversion into V<sub>2</sub>O<sub>5</sub> for lithium-ion batteries. *Angew. Chem.* **2013**, *125*, 2282-2286.

[41] Li, H. Q.; He, P.; Wang, Y. G.; Hosono, E.; Zhou, H. S. High-surface vanadium oxides with large capacities for lithium-ion batteries: from hydrated aerogel to nanocrystalline VO<sub>2</sub>(B), V<sub>6</sub>O<sub>13</sub> and V<sub>2</sub>O<sub>5</sub>. *J. Mater. Chem.* **2011**, *21*, 10999-11009.

[42] Sun, X.; Zhou, C. G.; Xie, M.; Hu, T.; Sun, H. T.; Xin, G. Q.; Wang, G. K.; George, S. M.; Lian, J. Amorphous vanadium oxide coating on graphene by atomic layer deposition for stable

- high energy lithium ion anodes. *Chem. Commun.* **2014**, *50*, 10703-10706.
- [43] Augustyn, V.; Dunn, B. Low-potential lithium-ion reactivity of vanadium oxide aerogels. *Electrochim. Acta* **2013**, *88*, 530-535.
- [44] An, Q. Y.; Wei, Q. L.; Mai, L. Q.; Fei, J. Y.; Xu, X.; Zhao, Y. L.; Yan, M. Y.; Zhang, P. F.; Huang S. Z. Supercritically exfoliated ultrathin vanadium pentoxide nanosheets with high rate capability for lithium batteries. *Phys. Chem. Chem. Phys.* **2013**, *15*, 16828-16833.
- [45] Zhao, D.; Zheng, L. R.; Xiao, Y.; Wang, X.; Cao M. H. Lithium storage in microstructures of amorphous mixed-valence vanadium oxide as anode materials. *ChemSusChem.* **2015**, *8*, 2212-2222.
- [46] Xu, Y.; Zheng, L.; Wu, C. Z.; Qi, F.; Xie, Y. New-phased metastable  $V_2O_3$  porous urchinlike micronanostructures: Facile synthesis and application in aqueous lithium ion batteries. *Chem. Eur. J.* **2011**, *17*, 384-391.
- [47] Chae, O. B.; Kim, J.; Park, I.; Jeong, H.; Ku, J. H.; Ryu, J. H.; Kang, K.; Oh, S. M. Reversible lithium storage at highly populated vacant sites in an amorphous vanadium pentoxide electrode. *Chem. Mater.* **2014**, *26*, 5874-5881.
- [48] Zhang, K.; Kim, H. J.; Shi, X. J.; Lee, J. T.; Choi, J. M.; Song, M. S.; Park, J. H. Graphene/acid coassisted synthesis of ultrathin  $MoS_2$  nanosheets with outstanding rate capability for a lithium battery anode. *Inorg. Chem.* **2013**, *52*, 9807-9812.
- [49] Nan, C. Y.; Lin, Z.; Liao, H. G.; Song, M. K.; Li, Y. D.; Cairns, E. J. Durable carbon-coated  $Li_2S$  core-shell spheres for high performance lithium/sulfur cells. *J. Am. Chem. Soc.* **2014**, *136*, 4659-4663.
- [50] Zhao, Y.; Gao, D. L.; Ni, J. F.; Gao, L. J.; Yang, J.; Li Y. One-pot facile fabrication of carbon-coated  $Bi_2S_3$  nanomeshes with efficient Li-storage capability. *Nano Res.* **2014**, *7*, 765-773.
- [51] Han, F.; Ma, L. J.; Sun, Q.; Lei, C.; Lu, A. H. Rationally designed carbon-coated  $Fe_3O_4$  coaxial nanotubes with hierarchical porosity as high-rate anodes for lithium ion batteries. *Nano Res.* **2014**, *7*, 1706-1717.
- [52] Dimesso, L.; Förster, C.; Jaegermann, W.; Khanderi, J. P.; Tempel, H.; Popp, A.; Engstler, J.; Schneider, J. J.; Sarapulova, A.; Mikhailova, D. et al. Developments in nanostructured  $LiMPO_4$  (M = Fe, Co, Ni, Mn) composites based on three dimensional carbon architecture. *Chem. Soc. Rev.* **2012**, *41*, 5068-5080.

- [53] Jang, B.; Park, M.; Chae, O. B.; Park, S.; Kim, Y.; Oh, S. M.; Piao, Y. Z.; Hyeon, T. Direct synthesis of self-assembled ferrite/carbon hybrid nanosheets for high performance lithium-ion battery anodes. *J. Am. Chem. Soc.* **2012**, *134*, 15010-15015.
- [54] Liu, B.; Zhang, J.; Wang, X. F.; Chen, G.; Chen, D.; Zhou, C. W.; Shen, G. Z. Hierarchical three-dimensional  $\text{ZnCo}_2\text{O}_4$  nanowire arrays/carbon cloth anodes for a novel class of high-performance flexible lithium-ion batteries. *Nano Lett.* **2012**, *12*, 3005-3011.
- [55] Zhou, L.; Zhao, D.; Lou, X. W. Double-shelled  $\text{CoMn}_2\text{O}_4$  hollow microcubes as high-capacity anodes for lithium-ion batteries. *Adv. Mater.* **2012**, *24*, 745-748.
- [56] Grugeon, S.; Laruelle, S.; Dupont, L.; Tarascon, J. M. An update on the reactivity of nanoparticles Co-based compounds towards Li. *Solid State Sci.* **2003**, *5*, 895-904.
- [57] Jiang, L.; Qu, Y.; Ren, Z. Y.; Yu, P.; Zhao, D. D.; Zhou, W.; Wang, L.; Fu, H. G. In situ carbon-coated yolk-shell  $\text{V}_2\text{O}_3$  microspheres for lithium-ion batteries. *ACS Appl. Mater. Interfaces* **2015**, *7*, 1595-1601.
- [58] Lee, J. E.; Yu, S. H.; Lee, D. J.; Lee, D. C.; Han, S. I.; Sung, Y. E.; Hyeon, T. Facile and economical synthesis of hierarchical carbon-coated magnetite nanocomposite particles and their applications in lithium ion battery anodes. *Energy Environ. Sci.* **2012**, *5*, 9528-9533.
- [59] Zheng, C.; Zhou, X. F.; Cao, H. L.; Wang, G. H.; Liu, Z. P. Synthesis of porous graphene/activated carbon composite with high packing density and large specific surface area for supercapacitor electrode material. *J. Power Sources* **2014**, *258*, 290-295.
- [60] Choi, S. H.; Kang, Y. C. Aerosol-assisted rapid synthesis of SnS-C composite microspheres as anode material for Na-ion batteries. *Nano Res.* **2015**, *8*, 1595-1603.
- [61] Choi, S. H.; Lee, J. K.; Kang, Y. C. Three-dimensional porous graphene-metal oxide composite microspheres: Preparation and application in Li-ion batteries. *Nano Res.* **2015**, *8*, 1584-1594.
- [62] Fei, H. L.; Peng, Z. W.; Li, L.; Yang, Y.; Lu, W.; Samuel, E. L. G.; Fan, X. J.; Tour, J. M. Preparation of carbon-coated iron oxide nanoparticles dispersed on graphene sheets and applications as advanced anode materials for lithium-ion batteries. *Nano Res.* **2014**, *7*, 502-510.
- [63] Pan, A. Q.; Wu, H. B.; Zhang, L.; Lou, X. W. Uniform  $\text{V}_2\text{O}_5$  nanosheet-assembled hollow microflowers with excellent lithium storage properties. *Energy Environ. Sci.* **2013**, *6*, 1476-1479.

## Electronic Supplementary Material (ESM)

### Carbon-supported and nanosheets-assembled vanadium oxide microspheres for stable lithium ion battery anodes

Chaojiang Niu<sup>1</sup>, Meng Huang<sup>1</sup>, Peiyao Wang<sup>1</sup>, Jiashen Meng, Xiong Liu, Xuanpeng Wang,  
Kangning Zhao, Yang Yu, Yuzhu Wu, Chao Lin, Liqiang Mai\*

State Key Laboratory of Advanced Technology for Materials Synthesis and Processing,  
Wuhan University of Technology, Wuhan 430070, China

<sup>1</sup>These authors contributed equally to this work.

\*Corresponding author E-mail address: [mlq518@whut.edu.cn](mailto:mlq518@whut.edu.cn)

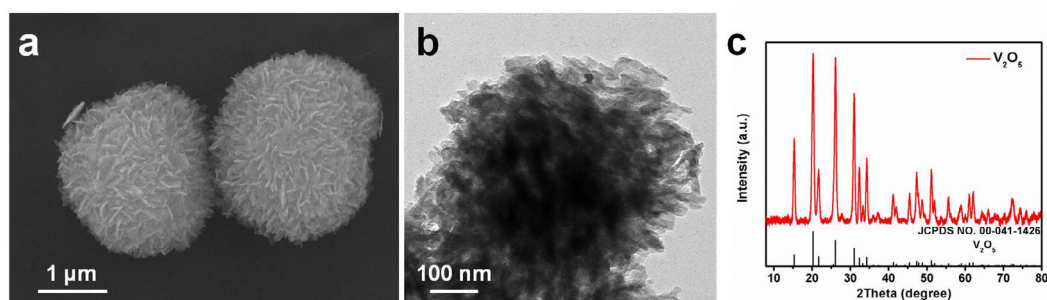


**Figure S1.** SEM image (a), TEM image (b) and XRD pattern (c) of V<sub>2</sub>O<sub>5</sub> microspheres assembled with nanosheets, which is obtained after sintering in air.

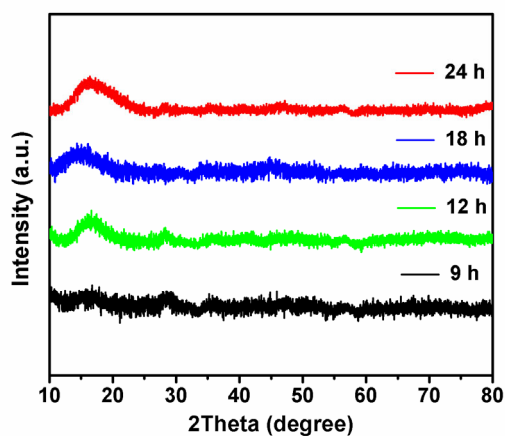


**Figure S2.** XRD patterns of carbon-supported and nanosheets-assembled amorphous vanadium oxide microspheres prepared at 9, 12, 18 and 24 h, respectively.

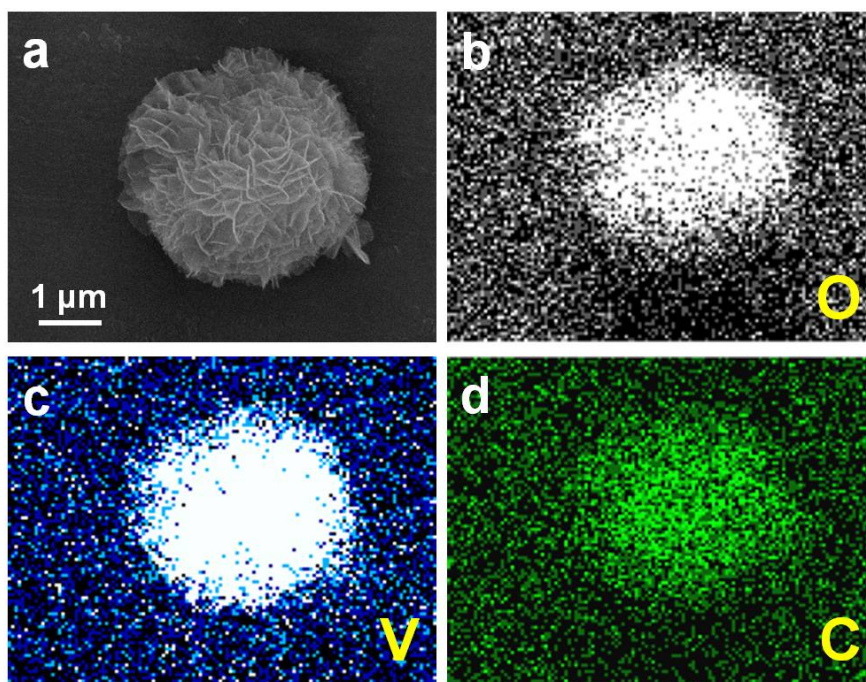


**Figure S3.** SEM image (a) and EDS elemental mappings of carbon-supported and nanosheets-assembled amorphous vanadium oxide microspheres. The elements of oxygen (b), vanadium (c), and carbon (d) are characterized, respectively.

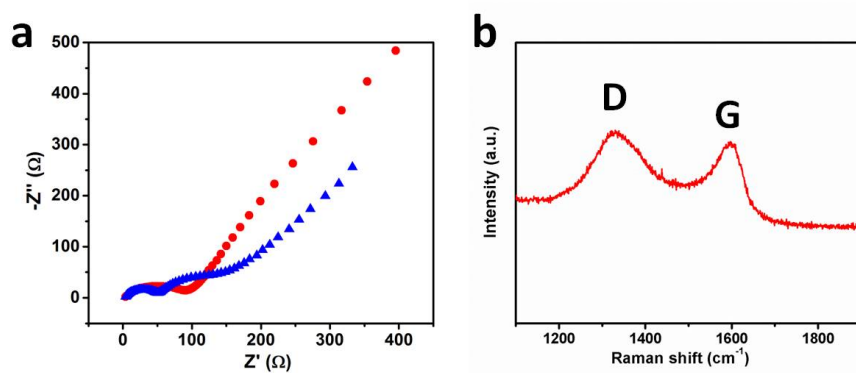


**Figure S4.** (a) AC impedance plots of amorphous vanadium oxide microspheres (red) and crystalline  $V_2O_3$  microspheres (blue), respectively. (b) Raman spectra of crystalline  $V_2O_3$  microspheres.

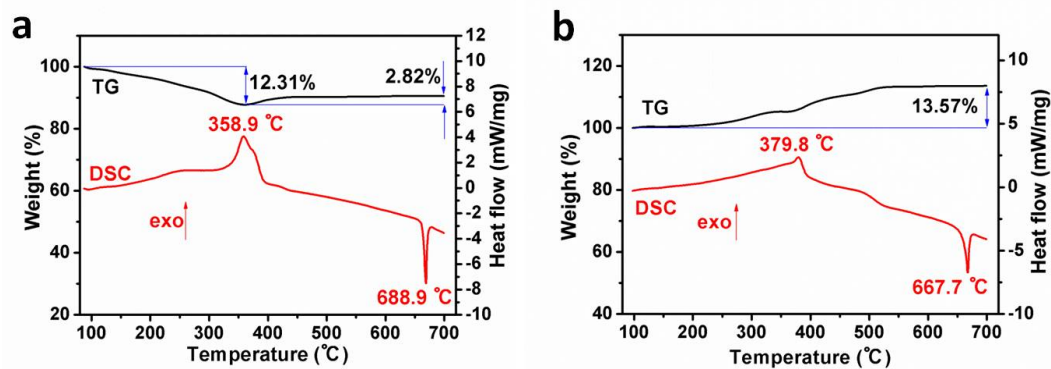


**Figure S5.** TG (black line) and DSC (red line) of amorphous vanadium oxide microspheres (a) and crystalline V<sub>2</sub>O<sub>3</sub> microspheres (b), respectively.

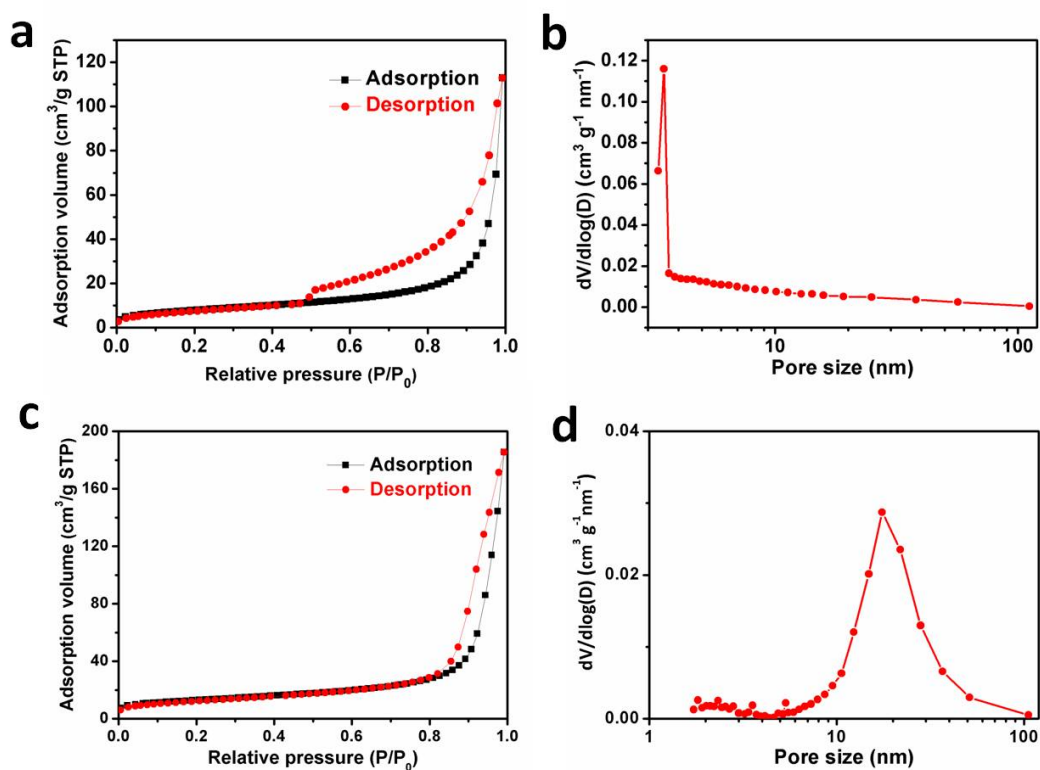


**Figure S6.** (a, b) Nitrogen adsorption-desorption isotherms and the corresponding pore size distribution of amorphous vanadium oxide microspheres; (c, d) Nitrogen adsorption-desorption isotherms and the corresponding pore size distribution of crystalline V<sub>2</sub>O<sub>3</sub> microspheres.

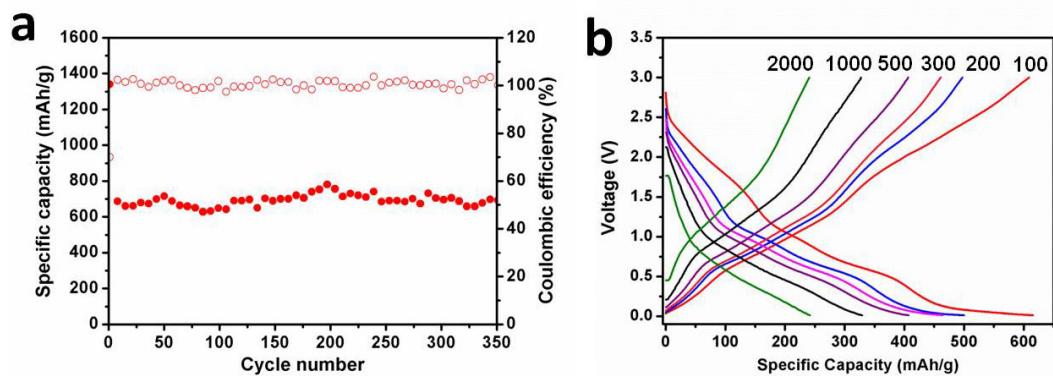


**Figure S7.** (a) Cycling performance of amorphous vanadium oxide microspheres tested at 100 mA/g. (b) Charge-discharge curves of amorphous vanadium oxide microspheres tested at different current densities ranging from 100 to 200, 300, 500, 1000, 2000 mA/g, respectively.

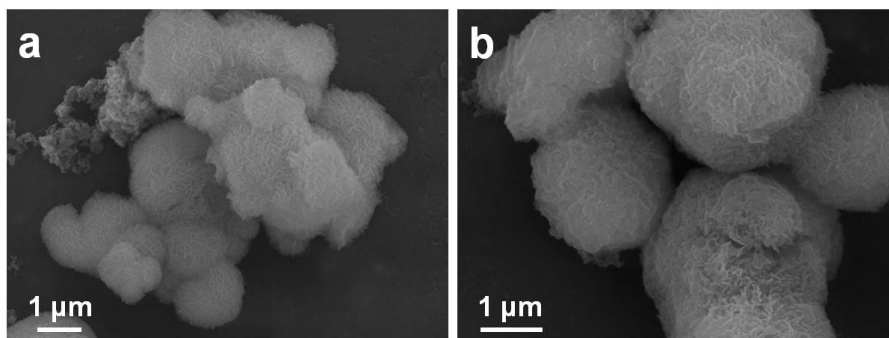


**Figure S8.** SEM images of amorphous vanadium oxide microspheres (a) and crystalline  $V_2O_3$  microspheres (b) after cycling 400 times at the current density of 200 mA/g.

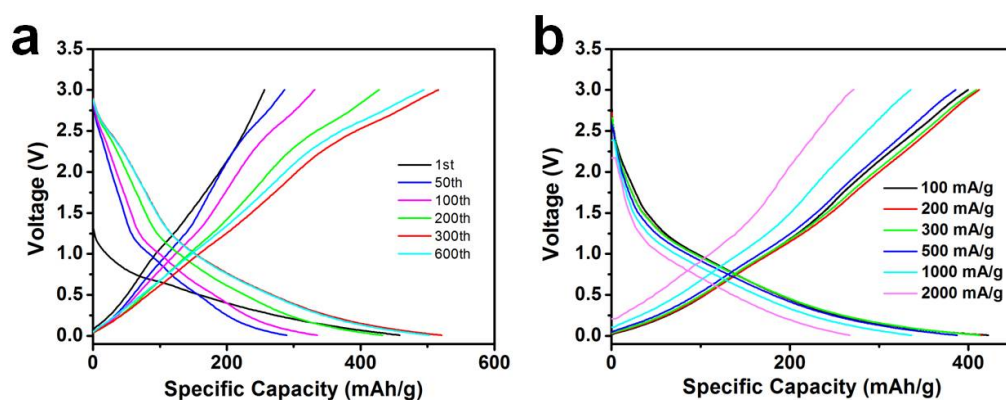


**Figure S9.** (a) The voltage profiles of crystalline  $V_2O_3$  microspheres tested at the current density of 200 mA/g. (b) The charge and discharge curves of crystalline  $V_2O_3$  microspheres tested at different current densities ranging from 100 to 2000 mA/g.

**Table S1.** The comparisons of our work and previously reports.

<b>Morphology</b>	<b>Voltage range (V)</b>	<b>Current density (mA/g)</b>	<b>The 2<sup>nd</sup> discharge capacity (mAh/g)</b>	<b>Cycle number</b>	<b>Capacity retention</b>	<b>Reference</b>
Carbon supported amorphous vanadium oxide microspheres	0.01-3.0	<b>2000</b>	345	<b>7000</b>	<b>95%</b>	<b>Our work</b>
Carbon supported V <sub>2</sub> O <sub>3</sub> microspheres	0.01-3.0	<b>2000</b>	245	<b>9000</b>	<b>98%</b>	
Amorphous vanadium coating on graphene	0.01-3.0	1000	500	200	101%	<i>Chem. Commun.</i> 2014, 50,10703.
Amorphous vanadium pentoxide	0.01-3.0	100	650	50	92%	<i>Chem. Mater.</i> 2014, 26, 5874.
V <sub>2</sub> O <sub>3</sub> -ordered mesoporous carbon	0.01-3.0	100	700	180	75%	<i>Carbon</i> , 2013, 62, 382.
V <sub>2</sub> O <sub>3</sub> /C nanocomposites	0.01-3.0	200	750	100	93%	<i>J. Power Sources</i> , 2014, 261, 184.